Article:
Wei, Y, Liu, Z, Guo, A et al. (6 more authors) (2021) Zein Colloidal Particles and Cellulose Nanocrystals Synergistic Stabilization of Pickering Emulsions for Delivery of β-Carotene. Journal of Agricultural and Food Chemistry, 69 (41). pp. 12278-12294. ISSN 0021-8561

https://doi.org/10.1021/acs.jafc.0c07800

Zein Colloidal Particles and Cellulose Nanocrystals Synergistic Stabilization of Pickering Emulsions for Delivery of β-Carotene

Yang Wei[1,2], Zikun Liu[1], Aixin Guo[1], Alan Mackie[2], Liang Zhang[1], Wenyan Liao[1], Like Mao[1], Fang Yuan[1], and Yanxiang Gao[1]*

[1] Beijing Key Laboratory of Functional Food from Plant Resources, College of Food Science & Nutritional Engineering, China Agricultural University, Box 112, No. 17 Qinghua East Road, Haidian District, Beijing 100083, P. R. China
[2] Food Colloids and Processing Group, School of Food Science and Nutrition, University of Leeds, Leeds LS2 9JT, U.K.

Abstract

In this study, we utilized different types of particles to stabilize β-carotene-loaded Pickering emulsions: spherical hydrophobic zein colloidal particles (ZCPs) (517.3 nm) and rod-shaped hydrophilic cellulose nanocrystals (CNCs) (115.2 nm). Either of the particles was incapable of stabilizing Pickering emulsions owing to their inappropriate wettability. When the mass ratio of ZCPs and CNCs was 1:4, the Pickering emulsion showed the best physical and photothermal stability. Compared to the ZCP-stabilized Pickering emulsion (9.29%), the retention rate of β-carotene in the Pickering emulsion costabilized by ZCPs and CNCs was increased to 60.23% after 28 days of storage at 55 °C. Confocal microscopy and cryoscanning electron microscopy confirmed that different types of particles could form a multilayered structure or induce the formation of an interparticle network. Furthermore, the complexation of ZCPs and CNCs delayed the lipolysis of the emulsion during *in vitro* digestion. The free fatty acid (FFA) release rate of Pickering emulsions in the small intestinal phase was reduced from 19.46 to 8.73%. Accordingly, the bioaccessibility of β-carotene in Pickering emulsions ranged from 9.14 to 27.25% through adjusting the mass ratio and addition sequence of distinct particles at the interface. The Pickering emulsion with the novel particle–particle complex interface was designed in foods and pharmaceuticals for purpose of enhanced stability, delayed lipolysis, or sustained nutrient release.

1. Introduction

The emulsions with adsorbed colloidal particles to stabilize the liquid–liquid interface are defined as Pickering emulsions. (1) Particles with intermediate wettability can facilitate the attachment of particles to the interface instead of the predominant distribution in the water or oil phase and increase the energy required for their desorption from the interface. Therefore, the particles attached at the interface confer the Pickering emulsion with a great ability to resist coalescence or Ostwald ripening. (2) Compared with the traditional emulsions stabilized by surfactants or polymers, Pickering emulsions show superior stability against coalescence, high internal phase proportion, stimuli responsiveness, and modulation of lipid digestion. Recently, a significant portion of the research has focused on the design of suitable particles to stabilize food-grade Pickering emulsions. The ingredients for making Pickering particles can be synthetic or natural polymeric materials, including surfactants, phospholipids, proteins, polyphenols, and polysaccharides. (3,4) However, the intricate production of the complex particles restricts their large-scale commercial application.

Within a real food matrix, particles, biosurfactants, and biopolymers often occur at the interface simultaneously, e.g., particles–biopolymers, particles–biosurfactants, and biopolymers–biosurfactants. (5−8) Because of the diversity in molecular structure, surface charge, addition sequence, and mass ratio between different surface-active components, the emulsions can form various microstructures depending on their interfacial composition. (9,10) Nevertheless, the interaction between different particles in the bulk phase or at the interface and their impact on the

stability and digestion behavior of Pickering emulsions have received limited attention. Sarkar et al. reported the production of Pickering emulsions using a composite layer of lactoferrin nanogel particles and inulin nanoparticles as a steric barrier to delay gastric digestion. (11) Various nanoparticles possess distinct hydrophilic/hydrophobic properties, morphologies, sizes, and surface charges. These characteristics affect the interparticle interaction and their adsorption and alignment at the interface, further impacting the interaction between the droplets. (12,13) Due to these unique properties, the complex interface composed of different particles can exhibit diverse structures that exert a vital role in stabilizing emulsions and delivering multiple nutraceuticals or drugs and have a promising potential in developing fat substitutes and porous materials through strengthening steric barriers to the interfacial disproportionation and coalescence. (13)

Cellulose nanocrystals (CNCs) are rod-shaped nanoparticles with high crystallinity, usually extracted from different bioresources. (14) CNCs are traditionally produced by sulfuric acid hydrolysis generated with anionic sulfate half-ester groups, which can prepare stable aqueous suspensions except under strong acid and high ionic strength. (15) The superiority of CNCs in food and pharmaceutical industries stems from their advantages such as high surface-area-to-volume ratio and excellent physicochemical stability. (16,17) The high aspect ratio provides CNCs with better mechanical properties and thermal stability, as well as unique rheological and optical properties, and also promotes the interconnection between CNCs during film formation and interfacial adsorption. Owing to these advantages and environmental sustainability, CNCs show promising applications in commercial formulations such as biomedicines, packaging materials, and personal care supplies. (18) Despite CNCs being recognized as hydrophilic (due to extensive hydroxylation), the highly ordered polymer chains endow the nanocrystals with amphiphilic properties due to a “hydrophobic edge”. (19−21) Unmodified CNCs can stabilize emulsions with a low surface charge density (22) because CNCs at the interface form a diluted mesh network within the interconnected droplets. (14,23) The combination of CNCs and other components for creating a stable emulsion has also been explored, such as polysaccharides, proteins, surfactants, and particles. (14,18) Unlike chemical modification of CNCs, these complex interfaces involving CNCs are generally formed by noncovalent interactions, thus adjusting surface hydrophobicity and interfacial structure in a more economically and environmentally friendly way. (24) As a dietary fiber that is indigestible in the upper digestive tract, CNCs can effectively inhibit lipid hydrolysis and ingestion when adsorbed on the surface of the lipid droplets, which is beneficial to prevent obesity and a variety of chronic diseases.

Zein, the major storage protein of maize, can be fabricated into zein colloidal particles (ZCPs) through self-assembly. (25) Although ZCP is regarded as a common Pickering stabilizer, the ZCP-stabilized Pickering emulsion is unstable due to the hydrophobicity of interfacial particles. (26) Many strategies have been proposed to control the interfacial wettability of zein-based particles through complexing with other ingredients, such as proteins, polysaccharides, and surfactants, which require a precise design and safety assessment. (27,28) In addition, the Pickering emulsion stabilized by ZCPs alone has a large interparticle space on the surface of the droplet, which results in the digestive components in the gastrointestinal tract that can be adsorbed to the droplet surface and cause lipid hydrolysis. Neither the hydrophobic ZCPs nor the hydrophilic CNCs have suitable wettability to stabilize Pickering emulsions alone. Due to the requirements of environmental sustainability and cumbersome production process, this study did not directly utilize chemical modification or prepare complex particles but the combination of ZCPs and CNCs was applied to prepare Pickering emulsions with particle–particle complex interfaces. The incorporation of CNCs could improve the hydrophobicity of interfacial particles and reduce the accessible surface area of emulsion droplets, which might enhance the stability of Pickering emulsions and restrict lipid digestion.

The objective of this study was to fabricate the Pickering emulsion costabilized by ZCPs and CNCs and to investigate the effects of the mass ratio and sequence of mixed particles on the properties of

Pickering emulsions with the complex particle–particle interface. We aimed to utilize distinct but imperfect particles with different characteristics to synergistically stabilize the oil–water interface instead of constructing composite particles. Subsequently, the physicochemical stability of β-carotene-loaded Pickering emulsions under different stresses was tested. *In vitro* gastrointestinal digestion of Pickering emulsions was determined, and the influence of interfacial composition on the lipolysis and bioaccessibility of β-carotene was investigated.

Materials and Methods

2.1. Materials

Zein (protein content, 91.3%), porcine pancreatic lipase type 2 (L3126), and bile salts (1:1 mixture of cholic acid and deoxycholic acid, 48305) were purchased from Sigma-Aldrich. The CNCs with a diameter of 5–20 nm and a length of 100–200 nm were obtained from Shanghai Science Nanotechnology Ltd. Cellulose nanocrystals (CNCs) were isolated by sulfuric acid hydrolysis of wood fibers. Medium-chain triglycerides (MCTs, Miglyol 812N) were purchased from Musim Mas (Medan, Indonesia). The β-carotene suspension (30% by mass β-carotene in sunflower oil) was supplied by Xinchang Pharmaceutical Company, Ltd. (Xinchang, Zhejiang, China). Absolute ethanol (99.99%), solid sodium hydroxide, and liquid hydrochloric acid (36%, w/w) were obtained from Eshowbokoo Biological Technology Co., Ltd. (Beijing, China). All other chemical agents were of analytical grade.

2.2. Preparation of ZCPs and CNCs

Zein colloidal particles (ZCPs) were fabricated by the solvent evaporation method. (29) Briefly, 3.0 g of zein was dissolved in 300 mL of 70% (v/v) aqueous ethanol solution and stirred at 600 rpm overnight at 25 °C. The ethanol in the solution was then removed at 45 °C for 25 min through rotary evaporation, and the remaining volume was set to be around 100 mL. The sample was diluted with pH-adjusted water (pH 4.0) to 150 mL. The ZCP suspension was centrifuged at 3000 rpm for 10 min to separate any large aggregates if any. Finally, the supernatant obtained was adjusted to pH 4.0 by 0.1 M HCl solution. The CNC suspension with the desired concentration was obtained by dispersing 1.5 g of CNC powder into 100 mL of deionized water and followed by ultrasonic treatment (10 min, 400 W) using a probe-type sonicator. The pH of the CNC suspension was adjusted to 4.0 by adding 0.1 M HCl or NaOH. In all samples, 50 mM NaCl was maintained in the aqueous phase to partially screen the surface charge of CNCs and promote their interfacial packing.

2.3. Characterization of ZCPs and CNCs

The particle size (Z-average size) and ζ-potential of ZCPs and CNCs were determined by a zetasizer (Nano-ZS90, Malvern Instruments Ltd., Worcestershire, U.K.). The type of cuvette used was DTS1060, and the scattering angle was 90°. Samples were diluted with distilled water to avoid multiple light scattering effects. Thereafter, the samples were adjusted to pH 4.0 to measure the particle size and ζ-potential. (29) All measurements were conducted in triplicate.

The morphologies of ZCPs and CNCs were captured with a Tecnai 200 transmission electron microscope (TEM, FEI Company, Eindhoven, Netherlands) at 60 kV accelerating voltage. The particle concentration was diluted to 0.2 mg/mL, and one drop of the dispersions was placed on a 200 mesh carbon-coated copper grid. Images with various magnifications were taken at 25 kV.

The morphological features of CNCs were observed with an atomic force microscope (AFM) (Veeco Company, Plainview, NY) equipped with an E-scanner. Tapping mode was used with a nominal spring constant of 20–100 Nm^{-1} and nominal resonance frequencies of 10–200 kHz. Briefly, 10 μL of sample was dropped onto freshly cleaved mica sheets mounted on sample disks and air-dried for more than 2 h before scanning.

The contact angles of ZCPs and CNCs were measured with an OCA 20 AMP (Dataphysics Instruments GmbH, Filderstadt, Germany). All of the measurements were conducted in triplicate and averaged. The freeze-dried samples were compressed to obtain tablets of 2 mm thickness and 13 mm diameter. Then, the tablets were placed into an optical glass cuvette, which contained MCT. Next, about 2 μL of deionized water was deposited on the surface of the tablets using a high-precision injector. After the equilibrium was attained, images of the drops formed were acquired using a digital camera and the $\theta^{o/w}$ value was calculated based on the LaPlace–Young equation. (27) Measurements were averaged over at least three drops.

2.4. Fabrication of β-Carotene-Loaded Pickering Emulsions

The β-carotene suspension (20 g) was first dissolved in MCT (180 g) to form the oil phase (3.0 wt % β-carotene).

2.4.1. Method I

The primary emulsion was fabricated by mixing different quantities of the ZCP (3.0%, w/w) suspension with 15 g of oil phase at 18 000 rpm by a blender (Ultra Turrax, model T25, IKA Labortechnic, Staufen, Germany). After the complete dispersion of the oil phase, the mixture was further homogenized for another 5 min. Secondary emulsions were fabricated by mixing the primary emulsion with different amounts of the CNC suspension (1.5%, w/w) and homogenized under the same condition. The total weight of ZCP and CNC suspensions was set to be 15 g, and the mass ratios of ZCPs to CNCs were designed to be 4:1, 2:1, 1:1, 1:2, and 1:4. The Pickering emulsions were termed 4Z1C, 2Z1C, 1Z1C, 1Z2C, and 1Z4C according to the mass ratios of ZCPs to CNCs. The pH of fresh emulsions was adjusted to 4.0.

2.4.2. Method II

The primary emulsion was fabricated by mixing different quantities of the CNC (1.5%, w/w) suspension with 15 g of oil phase at 18 000 rpm using a blender (Ultra Turrax, model T25, IKA Labortechnic, Staufen, Germany). After the complete dispersion of the oil phase, the mixture was further homogenized for another 5 min. Secondary emulsions were fabricated by mixing the primary emulsion with different quantities of the ZCP suspension (3.0%, w/w) and homogenized under the same condition. The total weight of ZCPs and CNCs suspensions was set to be 15 g, and the mass ratios of CNCs to ZCPs were designed to be 4:1, 2:1, 1:1, 1:2, and 1:4. The Pickering emulsions were termed 4C1Z, 2C1Z, 1C1Z, 1C2Z, and 1C4Z based on the mass ratios of CNCs to ZCPs. The pH of different Pickering emulsions was adjusted to 4.0 using 0.5 M HCl.

2.4.3. Control Groups

The Pickering emulsion was prepared by homogenizing 15.0 g of ZCP (3.0%, w/w) or CNC (1.5%, w/w) suspension with 15.0 g of oil phase through the same procedure and termed ZCPs or CNCs.

2.5. Droplet Size and ζ-Potential

The droplet size was determined after emulsion preparation for 12 h with a laser scattering size analyzer (LS230, Beckman Coulter, Brea, CA). The emulsions were diluted with deionized water and stirred to reach an obscuration rate between 8 and 12%. The optical parameters are applied as follows: a refractive index of 1.52 for MCT and absorption of 0.001, and a refractive index of 1.33 for the dispersant (deionized water). (8) The volume-area (D4,3) average diameter was calculated by eq 1

$$D_{4,3} = \frac{\sum n_i d_i^4}{\sum n_i d_i^3} \quad (1)$$

where n_i is the number of particles with diameter d_i.

The ζ-potential was measured according to the direction and velocity of droplet movement in a well-defined electric field using a Nano-ZS90 zetasizer (Malvern Instruments, Worcestershire, U.K.). The droplet concentration of emulsions was diluted to 0.005 wt % to minimize multiple scattering effects. The data were collected from at least 10 sequential readings per sample after 120 s of equilibration and calculated by the instrument based on the Smoluchowski model.

2.6. Rheological Properties

The rheological properties were measured at 25 °C with an AR-1500 rheometer (TA Instruments, West Sussex, U.K.) using a steel parallel plate (40 mm diameter, gap 0.100 mm). The samples were deposited onto the plate and allowed to reach temperature equilibrium for 5 min. For the steady-state flow measurement, the shear rate ranged from 0.1 to 100 s^{-1}, and the apparent viscosity (η) was collected. All of the dynamic tests were performed within the linear viscoelastic region, and a stress value of 1 Pa was chosen for the frequency test. The frequency was oscillated between 0.1 and 100 rad/s, and the strain was performed at 1%. (8) Both storage modulus (G′) and loss modulus (G″) were recorded as a function of frequency to determine whether the emulsion was strongly or weakly flocculated.

2.7. Physicochemical Stability of β-Carotene-Loaded Pickering Emulsions

2.7.1. Physical Stability

The physical stability of Pickering emulsions was analyzed with a LUMiSizer (L.U.M. 290 GmbH, Germany) based on the principle that centrifugation accelerates destabilization. Specifically, 1.8 mL of sample was centrifugated at 3000 rpm for 1 h at 25 °C with a fixed interval of 20 s.

2.7.2. Effect of Ultraviolet (UV) Radiation

The photostability of β-carotene under ultraviolet (UV) radiation was evaluated. (8) Briefly, the transparent glass vials containing 15 g of samples were transferred into transparent glass bottles in a controlled light cabinet (0.68 W/m2, 45 °C, QSUN Xe-1-B, Q-Lab Corporation, Ohio) for 4 h. The content of β-carotene was plotted against treatment time. The β-carotene in the emulsions was extracted three times with a mixture of 1 mL of ethanol and 3 mL of *n*-hexane. After adding the organic reagents, the mixed solution was vortexed for 2 min, and the supernatant was obtained after centrifugation at 3000 rpm for 10 min. The supernatant obtained after three extractions was collected and diluted to 10 mL. The β-carotene in the supernatant was further diluted to an appropriate concentration by n-hexane. Then, the absorbance at 450 nm was measured with a UV-1800 UV–vis spectrophotometer (Shimadzu, Kyoto, Japan). (30)

2.7.3. Effect of Thermal Treatment

The samples after 12 h storage at 25 °C were incubated at 90 °C for 60 min and then cooled down to 25 °C. (8) The droplet size, ζ-potential, and retention rate of β-carotene were determined after thermal treatment.

2.7.4. Effect of pH

The influence of pH on the stability of Pickering emulsions was tested following a previous report. (31) The prepared emulsions after 12 h storage at 25 °C were adjusted to pH levels of 2.5, 6.0, and 8.5 by 0.1 M NaOH or 0.1 M HCl.

2.7.5. Effect of Ionic Strength

Different weights of NaCl powder were mixed with the prepared emulsions after 12 h storage at 25 °C for 2 h. The NaCl concentrations of Pickering emulsions were adjusted to 10, 50, and 100 mM. (31)

2.7.6. Effect of Storage Time

After the preparation of Pickering emulsions, the fresh samples were stored at 55 °C for 4 weeks. The droplet size and retention rate of β-carotene in Pickering emulsions were measured at regular storage periods (1, 7, 14, 21, and 28 days).

2.8. Confocal Laser Scanning Microscopy (CLSM)

CLSM (Zeiss780, Oberkochen, Germany) was utilized to observe the microstructure of droplets. The emulsions were stained with a mixed fluorescent dye solution consisting of Nile blue (0.1% dissolved in absolute ethanol) and Nile red (0.1% dissolved in absolute ethanol). Then, the dyed emulsions were deposited on concave confocal microscope slides and gently covered with a coverslip. Nile blue was used to dye the ZCPs (red phase), and Nile red was applied to stain the oil phase (green phase). CLSM was operated with two laser excitation sources: an argon/krypton laser at 488 nm (Nile red) and a helium–neon laser (He–Ne) at 633 nm (Nile blue). (32)

2.9. Cryoscanning Electronic Microscopy (Cryo-SEM)

The sample was vitrified with liquid nitrogen and maintained at a very low temperature, which preserves the microstructure of Pickering emulsions in a frozen state and allows them to remain stable during the observation. (32,33) The samples were placed on an aluminum platelet, and then transferred to a cryopreparation system (PP3010T, Quorum Inc., Laughton, East Sussex, U.K.). The samples were freeze-fractured in the cryopreparation chamber and coated with platinum. Then, the images were taken through SEM (Helios NanoLab G3 UC, FEI, Hillsboro, OR). The analysis was conducted at a working distance between 3 and 5 mm with TLD detection at 2 kV.

2.10. *In Vitro* Gastrointestinal Digestion Analysis

An *in vitro* gastrointestinal model was applied in this study with some modifications. (34) All samples and solutions were maintained at 37 °C throughout the gastrointestinal digestion process.

2.10.1. Stomach Phase

The emulsion (20 mL) was mixed with 20 mL of simulated gastric fluid (SGF) containing 0.0032 g/mL pepsin to mimic gastric digestion. The pH was adjusted to 2.0, and the sample was then swirled at 150 rpm for 1 h.

2.10.2. Small Intestine Phase

Gastric digesta (20 mL) was transferred into a 100 mL glass beaker and then adjusted to pH 7.0. Thereafter, 20 mL of simulated intestinal fluid (SIF) containing 5 mg/mL bile salt, 0.4 mg/mL pancreatin, and 3.2 mg/mL lipase was mixed with digesta in the reaction vessel. The pH was adjusted to 7.0, and the samples were held under continuous stirring at 150 rpm for 2 h to mimic the small intestine digestion.

The degree of lipolysis was measured through the quantity of free fatty acids (FFAs) released. The quantity of 0.5 M NaOH required to neutralize the released FFA through lipid digestion was

determined by a pH-stat automatic titration unit (Metrohm, Switzerland, 916 Ti-Touch). The quantity of FFA released was determined as the percentage of FFA (%) released during the digestion time as described by eq 2 (35)

$$\%\ \mathrm{FFA} = \frac{V_{\mathrm{NaOH}} m_{\mathrm{NaOH}} M_{\mathrm{lipid}}}{2W_{\mathrm{lipid}}} \times 100 \quad (2)$$

where V_{NaOH} and m_{NaOH} represent the volume (L) and concentration (M) of the NaOH solution needed to neutralize the FFA, respectively, and W_{lipid} and M_{lipid} represent the initial mass (g) and molecular mass ($g \cdot mol^{-1}$) of the triacylglycerol oil, respectively.

The bioaccessibility of β-carotene was determined after intestinal digestion. (8) Part of digesta was processed by a high-speed centrifuge at 15 000 rpm for 60 min at 4 °C. The micelle phase containing the solubilized β-carotene was collected. The content of β-carotene extracted from the initial emulsion and micelle fraction was determined according to the method described in Section 2.7.2. The bioaccessibility (%) of β-carotene was calculated by eq 3

$$\mathrm{bioaccessibility}\ (\%) = \frac{C_{\mathrm{micelle}}}{C_{\mathrm{initial\ emulsion}}} \times 100 \quad (3)$$

where $C_{micelle}$ and $C_{initial\ emulsion}$ are the contents of β-carotene in the micelle fraction and the initial emulsion, respectively.

2.11. Statistical Analysis

All of the measurements were performed in triplicate, and the data obtained were average values of three determinations, which were subjected to statistical analysis of variance (ANOVA) with SPSS 18.0 (SPSS Inc., Chicago). Statistical differences were determined by one-way analysis of variance (ANOVA) with Duncan's posthoc test, and the least significant differences ($p < 0.05$) were accepted among the treatments.

3. Results and Discussion

3.1. Characteristics of ZCPs and CNCs

The ZCPs showed a spherical shape and high polydispersity in the particle size (Figure 1A). The slight aggregation between the particles was observed due to their inherent hydrophobicity. The Z-average size and ζ-potential of ZCPs were 517.3 ± 10.6 nm and 35.40 ± 1.06 mV, respectively. The large size of ZCPs restricted their rate of adsorption to the oil/water interface but endowed the resulting emulsion with excellent stability owing to high desorption energy, which was clarified by the classical literature. (36) The mean size of CNCs measured by DLS was 115.2 ± 1.3 nm, and the ζ-potential of CNCs was 41.24 ± 1.32 mV. Figure 1B,C demonstrates the TEM and AFM images of CNCs, respectively. The TEM image suggested that CNCs were stiff, needlelike particles with a nearly perfect crystalline structure, forming a compact network-type architecture, which was ascribed to the high aspect ratio of CNCs. The size and structure of CNCs observed were correlated with the morphology obtained by AFM. Figure 1D shows the complexation of ZCPs and CNCs in the bulk phase at a mass ratio of 2:1. The CNCs were intensively adsorbed on the surface of larger ZCPs, which was mainly attributed to the opposite charges carried by different types of particles, resulting in strong attraction between ZCPs and CNCs.

It is worth noting that CNCs formed a multilayered adsorption structure on the surface of ZCPs, and the interconnected CNC network extended into the aqueous phase to form bridges.

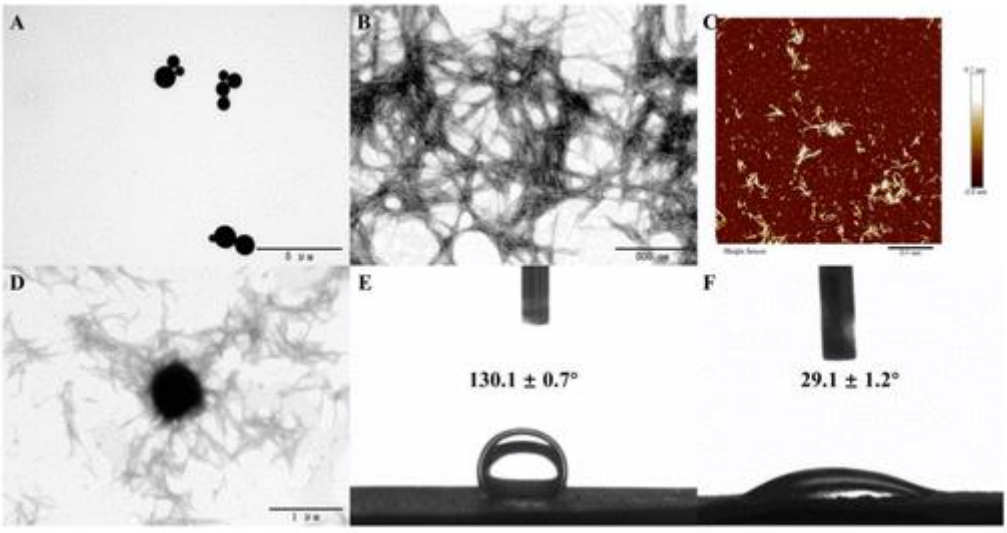

Figure 1. TEM images of ZCPs (A) and CNCs (B), AFM image of CNCs (C), TEM image of ZCP–CNC mixtures (D), and wettability of ZCPs (E) and CNCs (F)

Interfacial wettability is a vital indicator to assess the ability of particles to anchor at interfaces and generally expressed by the contact angle ($\theta_{o/w}$). (36) The $\theta_{o/w}$ of ZCPs was 130.1° (Figure 1E), indicating its strong hydrophobicity, which may cause severe droplet aggregation. (37) The result was consistent with the wettability of ZCPs fabricated by the solvent evaporation method according to a previous study. (27) The CNCs exhibited strong hydrophilicity with a $\theta_{o/w}$ of 29.1° due to the high number of hydroxyl groups (Figure 1F). This result indicated that CNCs were preferentially wetted by water rather than oil, which was consistent with the report of Hu et al. (14)

3.2. Droplet Size and ζ-Potential

As depicted in Figure 2A, the Pickering emulsion solely stabilized by ZCPs showed the largest droplet size ($D_{4,3}$) (5.11 ± 0.04 μm). The hydrophobic attraction between ZCPs at interfaces was stronger than steric and electrostatic repulsion, which induced the aggregation between droplets. The droplet size of the CNC-stabilized Pickering emulsion was 3.14 ± 0.02 μm, which was smaller than that of the ZCP-stabilized emulsion. Compared with ZCPs, the rodlike CNCs with a high aspect ratio could tangle with each other to form a bridge structure at the interface with higher stability. (24) Madivala *et al.* found that the higher concentrations of particles could interconnect to form a triangular mesh structure, thus constituting the network of the emulsion and restricting droplet coalescence. (38) Compared to ZCPs, elliptical particles (CNCs) showed higher efficiency in stabilizing emulsions. Moreover, the adsorption rate of smaller CNCs was higher than that of larger ZCPs, although the smaller size simultaneously reduced the desorption energy of CNCs attached at the interface. (36,39)

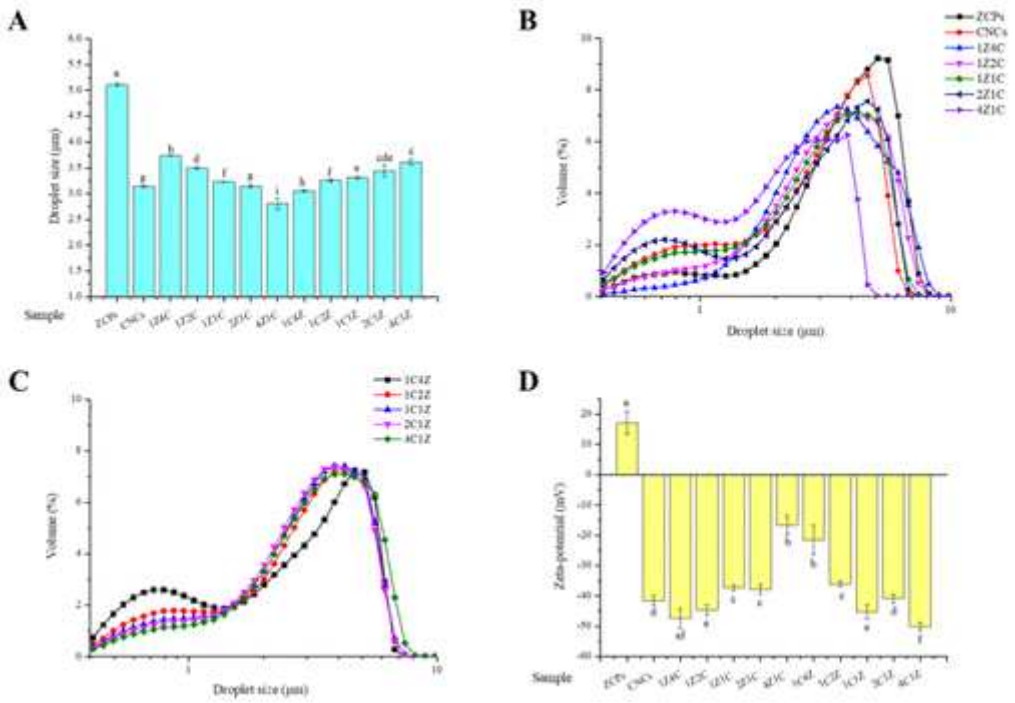

Figure 2. Mean droplet sizes of different Pickering emulsions (A), size distributions of Pickering emulsions stabilized by individual ZCPs and CNCs as well as the complex interface with ZCPs as an inner layer (B), size distributions of Pickering emulsions stabilized by the complex interface with CNCs as an inner layer (C), and ζ-potentials of different Pickering emulsions (D) [different superscript letters (a, b, c,...) in the figure indicate significant differences ($p < 0.05$)].

When ZCPs and CNCs coexisted at the interface, the addition sequence and mass ratio of different particles exhibited a significant influence on the droplet size. With the aid of CNCs, the droplet size of 4Z1C decreased to 2.81 ± 0.11 μm (Figure 2A). The presence of CNCs might reduce the hydrophobicity of ZCPs through adsorbing onto the particle surface, which might decrease the hydrophobic attraction between the droplets. Besides, Sarkar et al. (9) proposed an idealized model of monodispersed spherical particles at its highest surface coverage on the droplet surface; the size of the interparticle gaps would be $\frac{(\sqrt{3}-1)d}{2} \approx 189.3$ nm for ZCPs of size d = 517.3 nm. This was much larger than the mean size of CNCs (115.2 nm) measured by DLS. The smaller CNCs could fill up the interfacial gaps, which was also evidenced by cryo-SEM (Figure 10). A higher CNC content increased the droplet size of Pickering emulsions. The CNCs in the outer layer of droplets could be connected to each other and have resulted in droplet aggregation. On the contrary, in the Pickering emulsion with CNCs as an inner layer, the droplet size decreased continuously with increasing proportion of ZCPs. The CNCs were fixed at the interface along their length, which allowed their diffusion and reorganization. Therefore, a low concentration of CNCs was sufficient to cover the droplet surface of the emulsion and subsequently ZCPs could be adsorbed onto the CNC-laden interface to provide extra steric hindrance. Excessive CNCs could scarcely adsorb onto the droplet surface adequately and instead stretch into the aqueous phase, causing depletion flocculation, which was proved by the rheological properties of Pickering emulsions (Figure 3B).

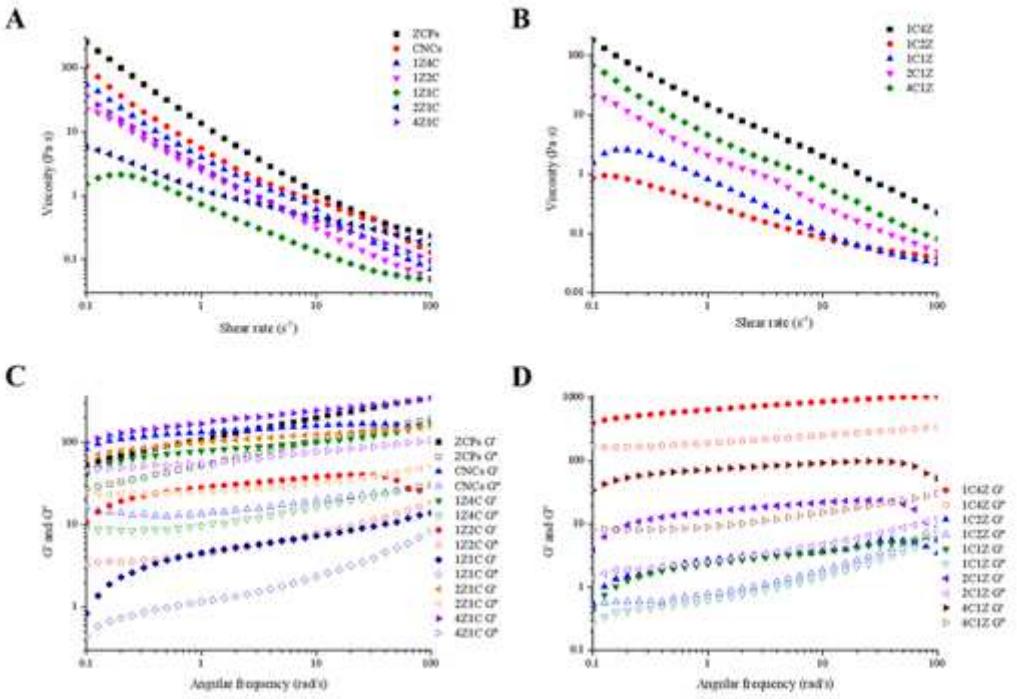

Figure 3. Apparent viscosity of Pickering emulsions using ZCPs as an inner layer and CNCs as an outer layer (A), apparent viscosity of Pickering emulsions stabilized by CNCs as an inner layer and ZCPs as an outer layer (B), viscoelasticity of Pickering emulsions stabilized by ZCPs as an inner layer and CNCs as an outer layer (C), and viscoelasticity of Pickering emulsions stabilized by CNCs as an inner layer and ZCPs as an outer layer (D).

Figure 2B shows the size distributions of Pickering emulsions stabilized by individual ZCPs and CNCs as well as the complex interface with ZCPs as an inner layer. The droplet size of the Pickering emulsion stabilized by ZCPs almost showed a single-peak distribution, while the size distribution of the Pickering emulsion stabilized by CNCs showed a small peak with the droplet size below 1 μm. This result meant that at higher particle concentrations, the wetting-induced self-assembly arose from CNCs in the continuous phase with subsequent aggregation. (21) Similarly, in the emulsions costabilized by whey protein and CNCs, the researchers revealed that unadsorbed CNCs occurred in the continuous phase at a higher level, which was confirmed by the droplet size distribution. (9) When the concentration of ZCPs in the inner layer was low, the small peak with a droplet size of less than 1 μm basically disappeared, but as the concentration of ZCPs increased, the intensity of the small peak gradually increased. This phenomenon interpreted that at a lower mass ratio of ZCPs to CNCs, CNCs could completely cover the surface of droplets. When the mass ratio of ZCPs to CNCs was higher, ZCPs might self-associate to aggregate due to their hydrophobic attraction, which was confirmed by the observation by CLSM (Figure 9). Zhang et al. reported the aggregation of unadsorbed particles in the continuous phase of the emulsion stabilized by pea protein microgels due to the attraction between particles. (40) A similar phenomenon was observed in Pickering emulsions stabilized by CNCs as an inner layer (Figure 2C). At a lower mass ratio of CNCs to ZCPs, the small peak with a droplet size of less than 1 μm appeared in the Pickering emulsion, indicating the aggregation of ZCPs in the continuous phase. With increasing mass ratio of CNCs to ZCPs, the large particle aggregates gradually disappeared. Figure 2D demonstrates the ζ-potential of different emulsions. The Pickering emulsions stabilized by ZCPs and CNCs solely carried a large magnitude of positive and negative charges, respectively. Therefore, ZCPs and CNCs could form a layer-by-layer structure on the droplet surface by electrostatic

deposition. With an increase in the mass ratio of ZCPs to CNCs, the absolute ζ-potential value decreased slightly due to the electrostatic complexation of ZCPs and CNCs.

3.3. Rheological Properties

3.3.1. Apparent Viscosity

The ZCP-stabilized Pickering emulsion showed the highest apparent viscosity among all of the emulsions (Figure 3A). As aforementioned, the interfacial particles (ZCPs) exhibited strong hydrophobicity, which caused serious droplet aggregation and even coalescence with higher viscosity. (41) Besides, the CNC-stabilized Pickering emulsion showed high viscosity, which was just behind that of the ZCPs. The wettability of particles is a key indicator indicating the propensity of an emulsion to aggregate via particle bridging. The hydrophilicity of CNCs promoted the particles entering the continuous phase, which decreased the attachment energy of particles and made them be shared between two droplets. (37) With the incorporation of CNCs into the ZCP-stabilized interface, the droplet size of Pickering emulsions with the particle–particle complex interface decreased and the emulsion viscosity also reduced greatly to a minimum (1Z1C). This phenomenon indicated that the addition of CNCs improved the hydrophobicity of ZCPs to reduce particle bridges. The CNCs were fully absorbed onto the interfacial gaps between ZCPs and enhanced the emulsion stability by strengthening the steric and electrostatic repulsion. Nevertheless, the increasing proportion of CNCs gradually elevated the viscosity of the emulsion. As aforementioned, CNCs preferentially formed particle bridges between droplets due to their hydrophilicity. Additionally, excessive CNCs might enter the continuous phase instead of adsorbing onto the interface, thus causing depletion flocculation.

When CNCs were applied as an inner layer, 1C4Z showed the highest viscosity (Figure 3B). This result was attributed to the hydrophobic interaction between ZCPs on the outer layer, which caused droplet aggregation and increased emulsion viscosity. (42) As the mass ratio of CNCs to ZCPs increased, the emulsion viscosity reduced rapidly to a minimum (1C2Z), interpreting that CNCs improved the stability of the emulsions and the hydrophobic attraction between ZCPs was reduced. When the proportion of CNCs was further increased, there was a continuous increase in the viscosity of the emulsions. The high level of CNCs tended to form particle bridges between droplets (37) and entered the continuous phase to promote depletion flocculation. (46)

3.3.2. Viscoelastic Properties

As illustrated in Figure 3, the G′ was higher than G″ of all of the Pickering emulsions, suggesting that an elastic particulate gel-like structure was generated. (31) The G′ value of the Pickering emulsion stabilized by ZCPs or CNCs alone was maintained at a high level (Figure 3C). This result unraveled that ZCPs and CNCs tended to form particle bridges between droplets after adsorption at the interface induced by their strong hydrophobic interaction or hydrophilicity. The bridging flocculation between droplets increased the G′ of the emulsions, exhibiting a solidlike behavior. With the adsorption of CNCs onto the ZCP-laden interface, the *G′* of 4Z1C increased slightly compared with that of the ZCP-stabilized Pickering emulsion. Nevertheless, as the mass ratio of ZCPs to CNCs decreased, the viscoelasticity of Pickering emulsions with the particle–particle complex interface reduced greatly and reached a minimum at 1Z1C. The presence of CNCs decreased the hydrophobicity of ZCPs and interfered with bridging flocculation between droplets. As the proportion of CNCs continued to increase, the viscoelasticity of the emulsions increased again, revealing that the excessive CNCs located in the outer layer or dispersed into the continuous phase, thus promoting depletion flocculation.

Figure 3D depicts the viscoelasticity of the Pickering emulsion with CNCs as an inner layer. At a higher mass ratio of CNCs to ZCPs, the adsorption of CNCs saturated the droplet surface, and part of ZCPs

entered the continuous phase to form larger aggregates. As the mass ratio of CNCs to ZCPs was decreased, the *G'* of the emulsions reduced continuously to be close to *G"*, which revealed that the Pickering emulsions exhibited a transition from solid to liquid characteristics with decreasing droplet size. The phenomenon proved that the combination of CNCs to ZCPs enhanced the repulsion between droplets through the interfacial layer and improved the emulsion stability synergistically. Notwithstanding, when the proportion of ZCPs in the outer layer was further increased, the *G'* of the emulsion greatly increased due to the hydrophobic attraction between ZCPs, thereby leading to droplet flocculation.

3.4. Environmental Stability

3.4.1. Physical Stability

As depicted in Figure 4A, the ZCP-stabilized Pickering emulsion showed the highest instability index. Compared with ZCPs, the CNC-stabilized Pickering emulsion showed better physical stability. Similar to ZCPs, at the low CNC content, 4Z1C was more unstable compared to other Pickering emulsions with ZCPs as an inner layer. With the mass ratio of ZCPs to CNCs decreasing, the emulsion stability improved until 1Z4C reached the minimum instability index. This result suggested that ZCPs and CNCs could synergistically stabilize Pickering emulsions with the complex interface, which was more stable than that of individual particle-stabilized emulsions. As the proportion of CNCs increased, the emulsion stability continued to be enhanced. Likewise, a similar phenomenon appeared for the physical stability of Pickering emulsions with CNCs as an inner layer (Figure 4B). Among all of the emulsions, 1C4Z showed the poorest physical stability due to the reduced electrostatic repulsion and strong hydrophobic attraction between droplets. Nevertheless, the higher mass ratio of CNCs to ZCPs enhanced the physical stability of emulsions. The synergistic effect between CNCs and ZCPs was ascribed to that CNCs increased the droplet surface coverage area and strengthened electrostatic repulsion. Meanwhile, ZCPs could increase the steric repulsion against droplet coalescence.

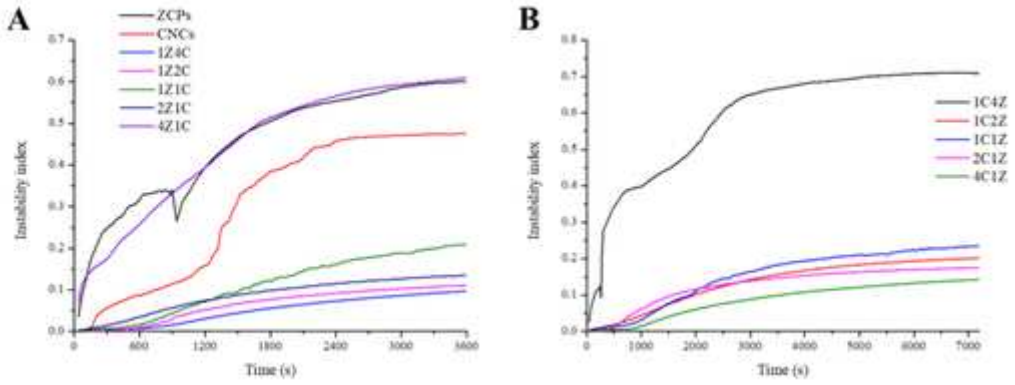

Figure 4. Physical stability of Pickering emulsions stabilized by ZCPs as an inner layer and CNCs as an outer layer (A) and physical stability of Pickering emulsions stabilized by CNCs as an inner layer and ZCPs as an outer layer (B).

3.4.2. Photostability

After 8 h of light exposure, β-carotene in the ZCP-stabilized Pickering emulsion degraded most quickly (Figure 5A), and the β-carotene content was reduced to 31.61 ± 2.24%. The large size of ZCPs made them unable to fully cover the droplet surface so that more light could enter into the droplets through the interfacial gaps between particles, leading to the degradation of β-carotene. (8) The retention rate of β-carotene in the CNC-stabilized Pickering emulsion was elevated to 72.43 ± 0.67%. Compared to

ZCPs, CNCs could form a more compact layer on the droplets, retarding the penetration of light and the degradation of β-carotene. It was observed that the introduction of the CNCs into polyvinyl alcohol films decreased their transparency with strong antiultraviolet ability. (44) Similar to the physical stability of the emulsions, the complex interface could not protect β-carotene effectively at a lower CNC concentration. For instance, the retention rate of β-carotene in 4Z1C was reduced to 53.20 ± 0.75%. As the mass ratio of CNCs to ZCPs increased, the photostability of β-carotene in the droplets was gradually enhanced, indicating that CNCs could protect β-carotene from chemical degradation more effectively than ZCPs. Among all of the emulsions, the retention rate of β-carotene in 1Z4C reached the maximum (80.43 ± 0.80%). Compared with a previous study, the Pickering emulsions costabilized by ZCPs and CNCs showed better performance than the emulsions costabilized by zein-propylene glycol alginate (PGA) composite nanoparticles and lactoferrin or rhamnolipid in terms of protection of β-carotene against UV radiation. (8) This phenomenon interpreted that the mixed particle-constituting interface could provide better protection to bioactive compounds under the exposure of light than that adsorbed by individual particles and emulsifiers or their combinations.

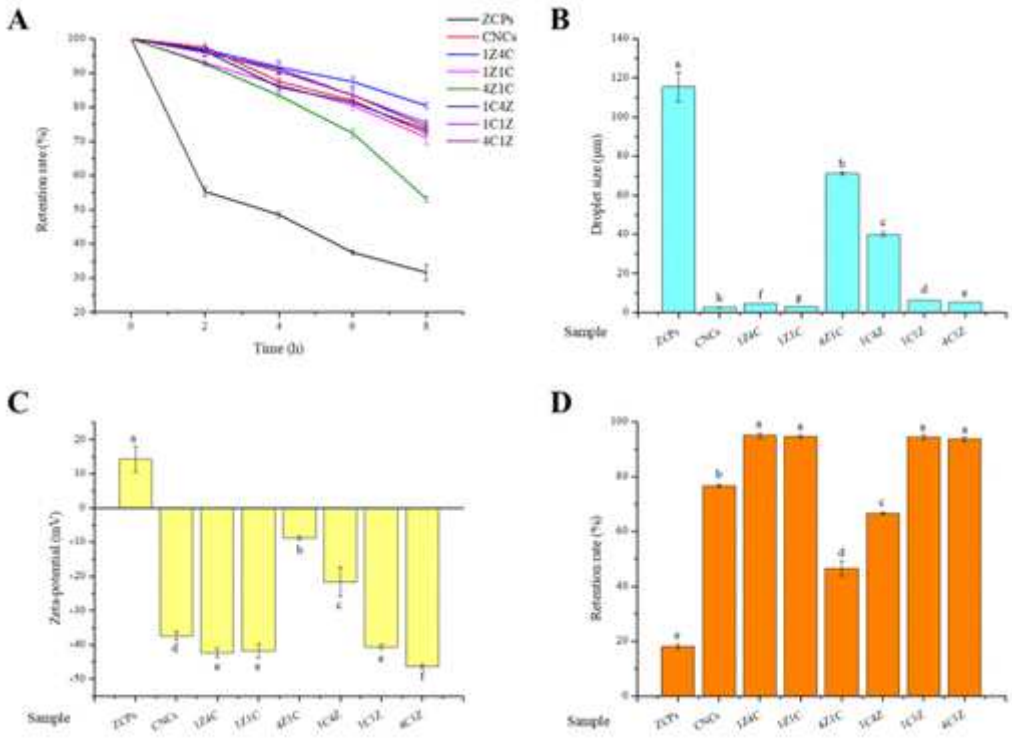

Figure 5. Photostability of β-carotene entrapped in Pickering emulsions (A) and influence of thermal treatment on droplet size (B) and ζ-potential (C) of Pickering emulsions and chemical stability of β-carotene (D) [different superscript letters (a, b, c,...) in the figure indicate significant differences (p < 0. 05)].

3.4.3. Thermal Stability

The droplet size of the ZCP-stabilized Pickering emulsion increased greatly to 115.37 ± 7.52 μm after thermal treatment (Figure 5B), revealing that the thermal treatment induced droplet coalescence. (42,43) Thermal treatment denatured the interfacial protein with the exposure of hydrophobic groups, which promoted the aggregation between the interfacial particles. Conversely, the CNC-stabilized Pickering emulsion remained stable after thermal treatment with constant droplet size, indicating that the introduction of CNCs endowed the interface with great thermal resistance owing to the stable structure of CNCs. (44) With the complexation of ZCPs and CNCs, there was an obvious

increase in the droplet size of Pickering emulsions at the low level of CNCs. As the proportion of CNCs was elevated, the thermal stability of Pickering emulsions improved, regardless of the order of addition of ZCPs and CNCs. The ζ-potential decreased slightly after thermal treatment, indicating that part of the particles desorbed from the interface. The absolute ζ-potential value of emulsion droplets was positively correlated with the degree of emulsion aggregation (Figure 5C), which suggested that electrostatic repulsion played an important role in the stabilization of Pickering emulsions.

After incubation at 90 °C for 60 min, β-carotene in the ZCP-stabilized Pickering emulsion showed the lowest retention rate (18.03 ± 0.92%) (Figure 5D). The CNC-stabilized Pickering emulsion showed much better protection for β-carotene (76.72 ± 0.58%) against thermal degradation due to the outstanding thermal stability of CNCs compared to protein nanoparticles. (44) Owing to the high aspect ratio, the CNCs might form a more compact interfacial layer with fewer gaps at the interface to reduce the transmission of heat. By forming the particle–particle complex interface, the thermal stability of β-carotene entrapped was further enhanced, except at the high ratio of ZCPs to CNCs. This phenomenon revealed the synergistic effect of ZCPs and CNCs in strengthening the thermal stability of Pickering emulsions.

3.4.4. Storage Stability

The storage stability of Pickering emulsions was tested for 4 weeks, and the size fluctuation of Pickering emulsions is demonstrated in Figure 6A. The ZCP-stabilized Pickering emulsion showed the largest increase of droplet size and was followed by 4Z1C and 1C4Z. Compared with ZCPs, the CNC-stabilized Pickering emulsion showed better storage stability with a small increase of droplet size. With a continuous increase in CNC concentration, the storage stability of Pickering emulsions with the mixed particle–particle interface was greatly improved. These results confirmed that the layer-by-layer structure of ZCPs and CNCs endowed the droplets with a rigid and robust interface to prevent emulsion coalescence, and therefore, different types of particles could synergistically stabilize the emulsions.

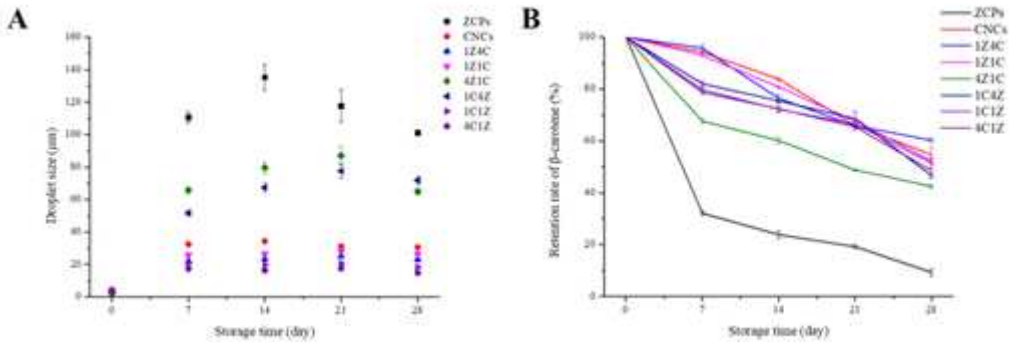

Figure 6. Effect of storage period on droplet size of Pickering emulsions (A) and retention rate of β-carotene entrapped in Pickering emulsions (B).

The chemical stability of β-carotene loaded in the emulsions was investigated during long-term storage (Figure 6B). The β-carotene in the ZCP-stabilized Pickering emulsion was the most unstable, with retention rates of 32.13 ± 0.78 and 9.29 ± 1.24% after 7 and 28 days, respectively. The β-carotene in the CNC-stabilized Pickering emulsion showed better stability, with 94.24 ± 0.56 and 54.69 ± 2.89% remaining after 7 and 28 days, respectively. However, the storage stability of β-carotene in the Pickering emulsion costabilized by ZCPs and CNCs was not improved compared with the CNC-stabilized Pickering emulsion. With the mass ratio of CNCs to ZCPs increasing, the retention rate of β-carotene

slightly increased, reaching the maximum in 1Z4C, manifesting that CNCs played a more important role in protecting β-carotene against chemical degradation through forming a denser interfacial layer.

3.4.5. pH Stability

The impact of different pH levels on the stability of Pickering emulsions with the particle–particle mixed interface was investigated (Figure 7). All of the emulsions remained stable at pH 2.0 except CNCs. The droplet size of the CNC-stabilized Pickering emulsion increased slightly due to the reduced electrostatic repulsion. With the pH being adjusted to 6, the droplet size of the ZCP-stabilized Pickering emulsion mostly increased, which was due to the pH close to the pI of zein. Other emulsions exhibited good stability at pH 6.0 except 4Z1C, presumable for the same reason. In a pH-neutral environment, the bilayered interfacial structure consisting of ZCPs and CNCs provided sufficient steric and electrostatic repulsion. The droplet size of the Pickering emulsion solely stabilized by ZCPs decreased obviously when the pH was elevated from 6 to 9. The increased charge strengthened the electrostatic repulsion between droplets. Although both ZCPs and CNCs carried negative charges and repelled each other, the Pickering emulsion with the particle–particle complex interface remained stable, which showed that the layer-by-layer interfacial structure composed of different particles was more stable than particle–biopolymer or particle–surfactant complex interfaces developed by our laboratory. (8,32) This phenomenon was mainly explained by that when the attraction between particle and biopolymer was not strong enough, the biopolymer could diffuse into the continuous phase, leading to depletion flocculation between droplets. (30,45,46)

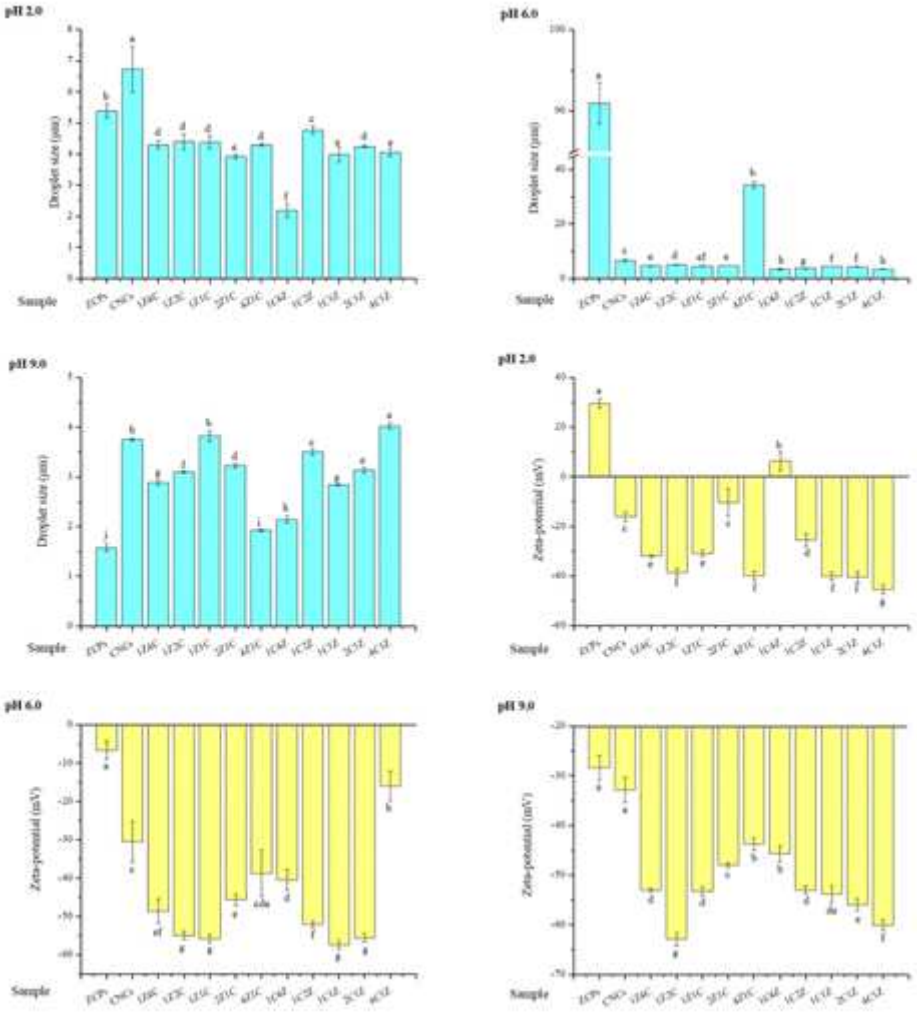

Figure 7. Confocal images of different Pickering emulsions with the lipid droplets in green surrounded by a layer of ZCPs in red [different superscript letters (a, b, c,...) in the figure indicate significant differences ($p < 0.05$)].

3.4.6. Ionic Strength Stability

The stability of Pickering emulsions was explored at different ionic strengths. The droplet sizes of all emulsions remained stable at 50 mM (Figure 8). Increasing NaCl concentration to 100 mM obviously increased the droplet size of the ZCP-stabilized Pickering emulsion due to the reduced electrostatic repulsion. Particularly, the droplet sizes of the CNC-stabilized Pickering emulsion and other emulsions with the mixed particle–particle interfaces decreased slightly at higher ionic strengths. This result may be attributed to that electrostatic shielding weakened the repulsion between CNCs, thereby promoting the adsorption of CNCs onto the interface. (24,47) When the ionic strength was increased to 200 mM, the droplet sizes of most emulsions increased slightly due to the reduced electrostatic repulsion. It is noteworthy that a larger increase of the droplet size appeared in ZCPs and 4Z1C, indicating that the Pickering emulsions were more unstable at a higher level of ZCPs. This phenomenon showed that it was difficult for ZCPs alone or the interfacial layer dominated by ZCPs to stabilize the Pickering emulsion at a higher ionic strength. As the electrostatic repulsion between droplets was reduced, the hydrophobic attraction between particles induced droplet flocculation. Nevertheless, at

a higher proportion of CNCs, ZCPs and CNCs exhibited a synergistic effect in stabilizing the Pickering emulsions.

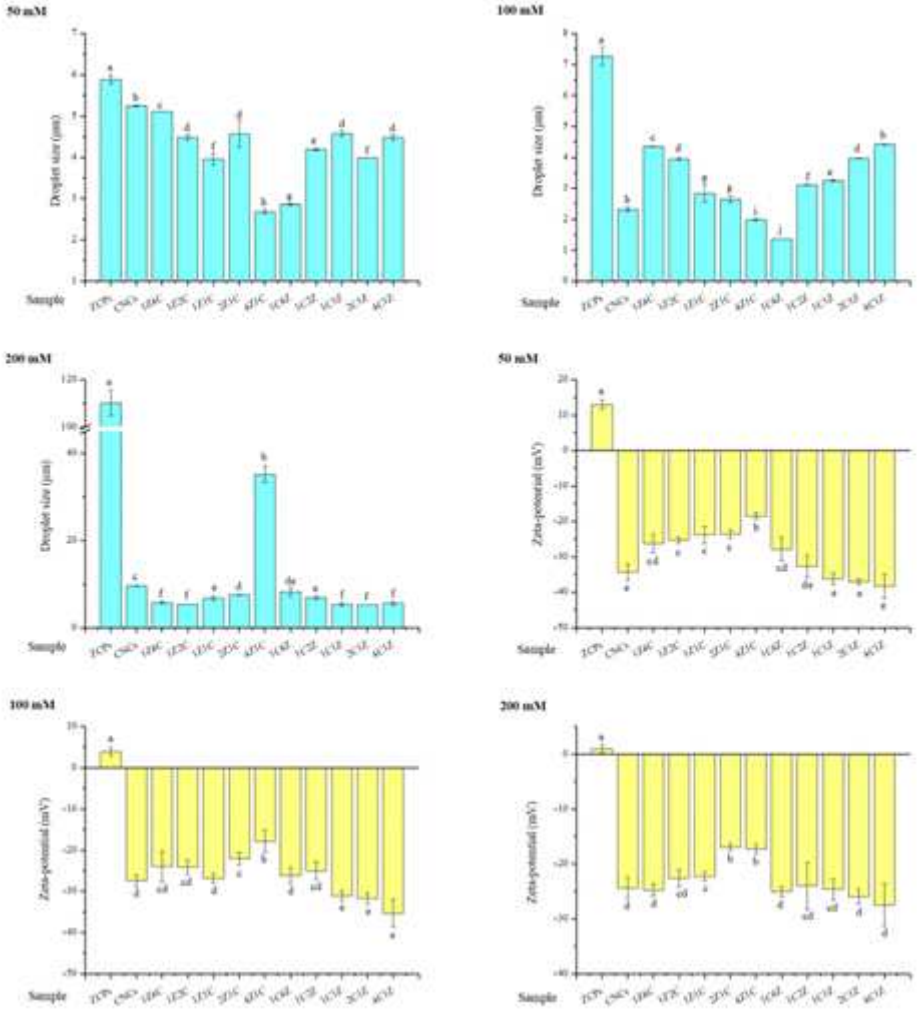

Figure 8. Impact of different pH values on the droplet size and ζ-potential of Pickering emulsions costabilized by ZCPs and CNCs [different superscript letters (a, b, c,...) in the figure indicate significant differences ($p < 0.05$)].

3.5. Morphological Observations

The droplets of the ZCP-stabilized Pickering emulsion were severely flocculated and bridged by ZCPs and their aggregates (Figure 9). In contrast, in the CNC-stabilized Pickering emulsion, the droplets were individually separated from each other without aggregation, indicating that CNCs were densely packed onto the droplet surface and provided the additional steric and electrostatic repulsion against the emulsion coalescence. When ZCPs were used as an inner layer and CNCs as an outer layer, a slight decrease appeared in the droplet size of Pickering emulsions with the particle–particle mixed interface at higher CNCs levels. Besides, the “red” ZCPs could not be observed at the interface through CLSM at a higher CNCs level, which suggested that CNCs displaced the part of ZCPs from the droplet surface. With the mass ratio of ZCPs to CNCs rising, there was an obvious aggregation in the emulsions with larger droplet sizes. It was observed that ZCPs began to adsorb on the interface and aggregate, and even enter the continuous phase, which was consistent with the size distributions of Pickering emulsions (Figure 2B). This phenomenon indicated that ZCPs aggregated with each other into larger particle aggregates due to hydrophobic interaction, reducing the efficiency of covering on the

interface. Meanwhile, a higher proportion of ZCPs could generate more bridges between droplets, further forming a network structure.

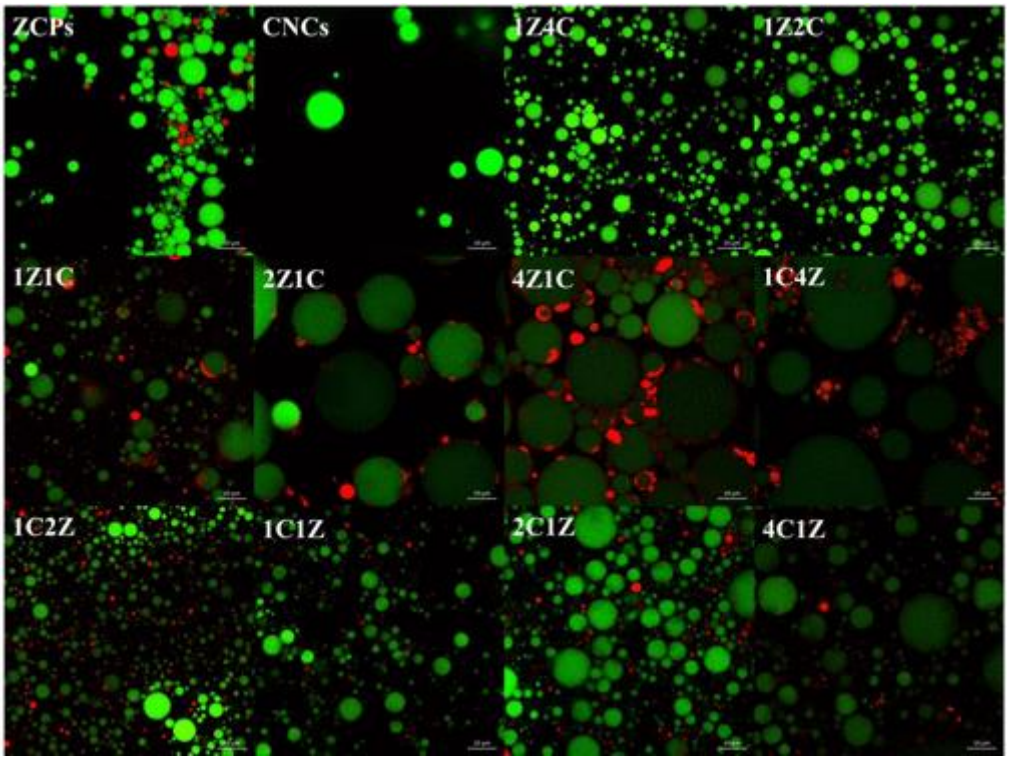

Figure 9. Influence of different ionic strengths on the droplet size and ζ-potential of Pickering emulsions costabilized by ZCPs and CNCs [Different superscript letters (a, b, c,...) in the figure indicate significant differences ($p < 0.05$)].

When CNCs were utilized as an inner layer, it was hard to distinguish the protein particle layer on the droplet surface (Figure 9). Alternatively, when the proportion of ZCPs was high, hydrophobic ZCPs aggregated into larger clusters in the continuous phase, which might cause depletion flocculation. With an increase of CNC proportion, the droplet size of Pickering emulsions decreased and then increased slightly. This result showed that when rod-shaped CNCs were fully adsorbed on the droplet surface, they could provide sufficient steric and electrostatic repulsion to retard coalescence. At a higher mass ratio of CNCs to ZCPs, excessive CNCs might enter the continuous phase, inducing depletion flocculation between droplets. (24,47)

Cryo-SEM can be applied to observe the microstructure of Pickering emulsions with the mixed particle–particle interface (Figure 10), which allows it to remedy the weakness of the observations through CLSM. The distribution of ZCPs on the droplet surface was obviously sparse, and they could not occupy the droplet surface adequately and prevent droplet aggregation. Additionally, due to the larger size and strong hydrophobicity, ZCPs tended to aggregate and bridge in the interfacial or the bulk phase, which reduced the packing efficiency of the particles on the droplet surface. Compared to the ZCP-stabilized Pickering emulsion, the rod-shaped CNCs were densely distributed at the interface to form a rigid layer, inhibiting coalescence more efficiently. With the complexation of ZCPs and CNCs, it was observed that loosely distributed ZCPs with a larger size and closely packed CNCs with smaller size were coadsorbed at the interface. At a lower proportion of ZCPs, a small amount of ZCPs was sparsely dispersed on the droplet surface, while densely distributed CNCs could be observed on the rest of the droplet surface. As the level of ZCPs increased, more and larger ZCPs with uneven particle

size would appear, indicating that ZCPs tended to aggregate at the interface due to the strong hydrophobicity. The phenomenon was consistent with the observation through CLSM. It is worth noting that CNCs could be adsorbed to the surface of ZCP aggregates, which might change the properties of the interfacial particles. Regardless of the addition sequence, the effect of the mass ratio of ZCPs and CNCs on the interfacial structure was basically consistent.

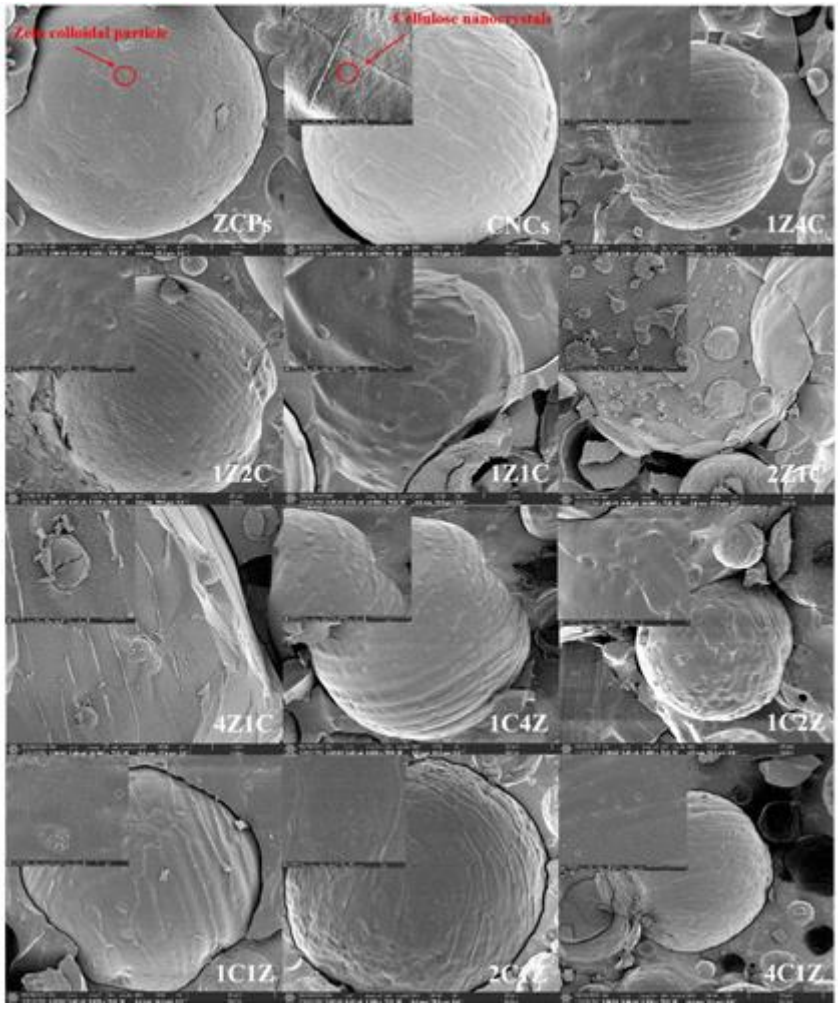

Figure 10. Cryo-SEM microstructures of different Pickering emulsions.

3.6. *In Vitro* Digestion of Pickering Emulsions

3.6.1. Lipid Digestion

As depicted in Figure 11A, the ZCP-stabilized Pickering emulsion showed the highest FFA release (19.46%), although it was lower than traditional emulsions stabilized by biopolymers or surfactants. (10) Meanwhile, the CNC-stabilized Pickering emulsion showed a much lower FFA release (12.31%). The particle stabilizers were difficult to be displaced by bile salts or lipases due to the high desorption energy, which could restrict the lipid digestion efficiently. Nevertheless, in this study, ZCPs could hardly cover the interface adequately due to particle aggregation, and therefore, there existed substantial interfacial gaps between ZCPs. (8) The cryo-SEM images showed the droplets surrounded by a compact layer of CNCs, demonstrating the propensity of the CNCs to restrict the contact of bile salts and lipases/colipases with the droplet surface (Figure 10). These results suggested that compared with the protein particles that were easily affected by enzymes conditions, CNCs were more promising as Pickering emulsion stabilizers in controlling lipid digestion. (24) As a control, the MCT oil was

digested under the GIT, which only released 5.38% FFA in the intestinal phase. Without the addition of effective emulsifiers, the triglycerides were not dispersed and stabilized before entering the GIT, which reduced the specific surface area of the lipid phase and limited the contact of droplets with lipases.

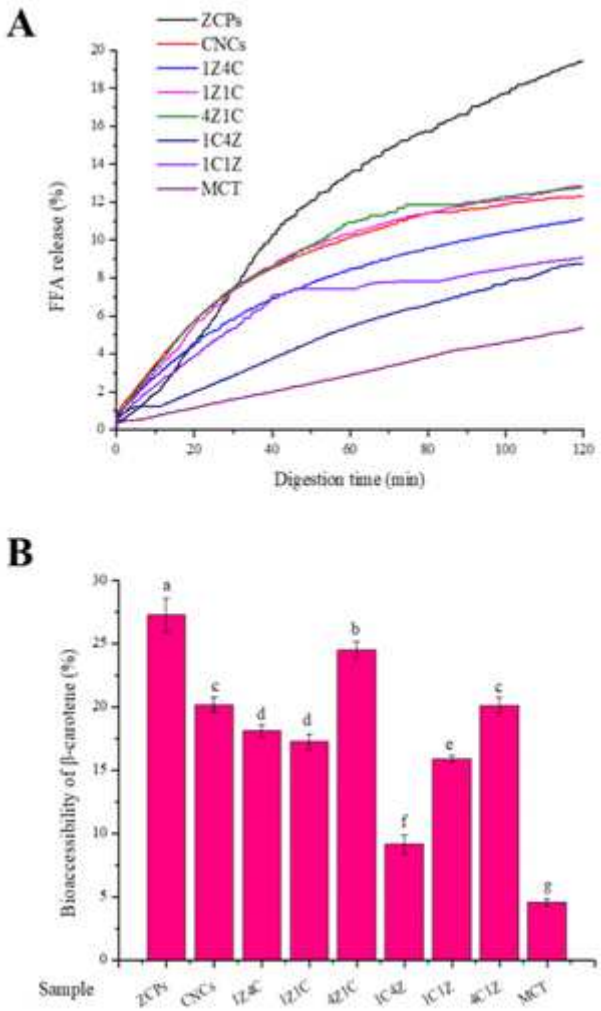

Figure 11. Digestion time dependence of FFA release (%) from different Pickering emulsions (A) and bioaccessibility of β-carotene entrapped in different Pickering emulsions (B) [different superscript letters (a, b, c,...) in the figure indicate significant differences ($p < 0.05$)].

With the incorporation of CNCs, the lipolysis of the ZCP-stabilized Pickering emulsion was effectively retarded. The FFA release rate of 4Z1C was reduced to 12.88% at a low proportion of CNCs. CNCs could enter into the uncovered areas at the ZCP-stabilized interface, which blocked the gaps at the ZCP-coated interface and limited the access of bile salts and lipases to the interface. (48) With a continuous increase in CNC proportion, the FFA release of Pickering emulsions was slightly decreased and similar to the CNC-stabilized interface. In addition to the adsorption onto the gaps between ZCPs at the interface, excessive CNCs could combine with ZCPs and cover the surface of ZCPs through electrostatic and hydrophobic attraction, which limited the proteolysis and detachment of protein particles. As the outer layer, CNCs adsorbed to the droplet surface also reduced the proximity of the negatively charged bile salts and lipase through charge repulsion, which restricted interfacial displacement. It was

reported that the bridging of CNCs to the protein-covered droplets could reduce the exposed surface area of the droplets for lipid digestion. (9)

When CNCs were utilized as an inner layer, the FFA release of Pickering emulsions with the particle–particle complex interfaces was much lower than that with ZCPs as the inner layer. Compared with the Pickering emulsion stabilized by CNCs alone, as the proportion of ZCPs was increased, the degree of lipid hydrolysis of the emulsions gradually decreased. The continuous increase of ZCPs reduced the release rate of FFA to 11.36, 9.08, and 8.73% for 4C1Z, 1C1Z, and 1C4Z, respectively. Compared with the ZCP-stabilized interface, the irreversibly strong adsorption of CNCs onto the droplet surface restricted the penetration of bile salts and lipases more effectively owing to the formation of a densely packed shell with CNCs as an inner layer. Nevertheless, it was at odds with previous studies on the CNC-stabilized Pickering emulsion that reported that the degree of inhibiting lipolysis was improved with an increase of CNC concentration. Interestingly, in this case, decreasing the mass ratio of CNCs to ZCPs strengthened the ability of complex interfaces to retard lipolysis, indicating that CNCs and ZCPs could synergistically delay lipid digestion. This phenomenon could be explained by the positive charge of ZCPs, which could produce strong electrostatic complexation between ZCPs and negatively charged bile salts, thereby reducing the approach and displacement of bile salts at the interface. The CLSM images showed that the addition of ZCPs as an outer layer caused droplet flocculation in Pickering emulsions (Figure 9). The relatively large droplet size (low specific surface area) reduced the exposed surface area accessible to bile salts. Moreover, the higher viscosity limited the diffuse and adsorption of bile salts and lipase/colipase and delayed the digestion (Figure 3B). (41,49)

3.6.2. Bioaccessibility of β-Carotene

As a prerequisite for determining the bioaccessibilities, the release and solubilization of fat-soluble nutrients mainly occur in the digestion stage of the small intestine and are dependent on a variety of exogenous factors, such as molecular property, food matrix, processing, and interfacial composition. (50) In the present study, the β-carotene bioaccessibility of the ZCP-stabilized emulsion was 27.25% and significantly higher than those of other emulsions (Figure 11B), which was consistent with its highest FFA release. Substances such as FFAs and bile salts facilitated the formation of mixed micelles, and lipolysis promoted the ability of mixed micelles to dissolve nutrients. Meanwhile, indigestible CNCs formed a densely packed interface that restricted the access of bile salts and lipases to lipid droplets, which effectively reduced the FFA release and β-carotene bioaccessibility (20.14%). As a control, the nonemulsified oil containing β-carotene was mixed with simulated small intestine fluids and the lowest β-carotene bioaccessibility was found in MCT (4.56%). In the absence of exogenous emulsifiers, the bile salts were incapable of stabilizing emulsions, thus causing droplet flocculation and coalescence. The large droplet size resulted in a low specific surface area available for lipase/colipase attachment, which inhibited the FFA release and decreased the β-carotene bioaccessibility. The interfacial composition exhibited a profound influence on the Pickering emulsions with the particle–particle composite interface. When ZCPs were used as an inner layer and CNCs as an outer layer, the bioaccessibility of β-carotene was continuously reduced with an increase in CNC proportion. This result was mainly because CNCs could fill the interfacial gaps in ZCP-covered droplets and limit the access of bile salts and lipases to reach the droplet surface. (48) Besides, CNCs adsorbed limited the proximity of the negatively charged bile salts and lipase through charge repulsion. The declination in the FFA release consequently reduced the formation of mixed micelles and the transfer of nutrients. Meanwhile, the addition of ZCPs onto the CNCs-stabilized emulsion decreased the bioaccessibility of β-carotene from 20.13% (4C1Z) to 9.14% (1C4Z). This result could be attributed to that the negatively charged ZCPs strengthened repulsion to negatively charged bile salts at the neutral pH under the intestinal condition, which not only restricted the approaching of bile salts at the interface but also reduced the participation of bile salts in forming mixed micelles. These mechanisms explained the

lower bioaccessibility of β-carotene in the Pickering emulsions with CNCs as the inner layer and ZCPs as the outer layer, and the bioaccessibility of β-carotene increased with a decrease in the level of ZCPs.

4. Conclusions

Spherical hydrophobic ZCPs and rod-shaped hydrophilic CNCs were combined to stabilize Pickering emulsions for delivery of β-carotene. Through the layer-by-layer deposition method, the physicochemical stability of Pickering emulsions was tailored by adjusting the mass ratio and addition sequence of different particles. Among all of the emulsions, when the mass ratio of ZCPs to CNCs was 1:4, the Pickering emulsions with the particle–particle complex interface showed the best stability. Meanwhile, when CNCs were used as an inner layer and ZCPs were used as an outer layer, they could synergistically inhibit the lipolysis of Pickering emulsions in gastrointestinal digestion through steric and electrostatic interaction while maintaining higher bioaccessibility of β-carotene. The experimental results confirmed that retardance of fat digestion was most profound when CNCs were used as the inner layer. The novel Pickering emulsion with the particle–particle complex interface could be incorporated in foods as well as pharmaceuticals for inhibition of lipid hydrolysis or precise delivery of nutraceuticals.

Notes

The authors declare no competing financial interest.

Acknowledgments

The research was funded by the National Natural Science Foundation of China (No. 31871842). The authors are grateful to Tsinghua University Branch of China National Center Protein Sciences (Beijing, China) for providing the facility support of Cryo-SEM with the aid of Xiaomin Li.

References.

1 Binks, B. P.; Lumsdon, S. O. Influence of Particle Wettability on the Type and Stability of Surfactant-Free Emulsions. Langmuir 2000, 16, 8622– 8631, DOI: 10.1021/la000189s

2 Xiao, J.; Li, Y.; Huang, Q. Recent Advances on Food-Grade Particles Stabilized Pickering Emulsions: Fabrication, Characterization and Research Trends. Trends Food Sci. Technol. 2016, 55, 48– 60, DOI: 10.1016/J.TIFS.2016.05.010

3 Zou, Y.; Guo, J.; Yin, S.-W.; Wang, J.-M.; Yang, X.-Q. Pickering Emulsion Gels Prepared by Hydrogen-Bonded Zein/Tannic Acid Complex Colloidal Particles. J. Agric. Food Chem. 2015, 63, 7405– 7414, DOI: 10.1021/acs.jafc.5b03113

4 Wei, Y.; Yu, Z.; Lin, K.; Yang, S.; Tai, K.; Liu, J.; Mao, L.; Yuan, F.; Gao, Y. Fabrication, Physicochemical Stability, and Microstructure of Coenzyme Q10 Pickering Emulsions Stabilized by Resveratrol-Loaded Composite Nanoparticles. J. Agric. Food Chem. 2020, 68, 1405– 1418, DOI: 10.1021/acs.jafc.9b06678

5 Binks, B. P.; Desforges, A.; Duff, D. G. Synergistic Stabilization of Emulsions by a Mixture of Surface-Active Nanoparticles and Surfactant. Langmuir 2007, 23, 1098– 1106, DOI: 10.1021/la062510y

6 Dickinson, E. Mixed Biopolymers at Interfaces: Competitive Adsorption and Multilayer Structures. Food Hydrocolloids 2011, 25, 1966– 1983, DOI: 10.1016/J.FOODHYD.2010.12.001

7 McClements, D. J.; Gumus, C. E. Natural Emulsifiers—Biosurfactants, Phospholipids, Biopolymers, and Colloidal Particles: Molecular and Physicochemical Basis of Functional Performance. Adv. Colloid Interface Sci. 2016, 234, 3– 26, DOI: 10.1016/j.cis.2016.03.002

8 Wei, Y.; Tong, Z.; Dai, L.; Wang, D.; Lv, P.; Liu, J.; Mao, L.; Yuan, F. Influence of Interfacial Compositions on the Microstructure, Physiochemical Stability, Lipid Digestion and β -Carotene Bioaccessibility of Pickering Emulsions. Food Hydrocolloids 2020, 104, 105738 DOI: 10.1016/j.foodhyd.2020.105738

9 Sarkar, A.; Li, H.; Cray, D.; Boxall, S. Composite Whey Protein–Cellulose Nanocrystals at Oil-Water Interface: Towards Delaying Lipid Digestion. Food Hydrocolloids 2018, 77, 436– 444, DOI: 10.1016/j.foodhyd.2017.10.020
10 Sarkar, A.; Zhang, S.; Holmes, M.; Ettelaie, R. Colloidal Aspects of Digestion of Pickering Emulsions: Experiments and Theoretical Models of Lipid Digestion Kinetics. Adv. Colloid Interface Sci. 2019, 263, 195– 211, DOI: 10.1016/j.cis.2018.10.002
11 Sarkar, A.; Ademuyiwa, V.; Stubley, S.; Esa, N. H.; Goycoolea, F. M.; Qin, X.; Gonzalez, F.; Olvera, C. Pickering Emulsions Co-Stabilized by Composite Protein/Polysaccharide Particle-Particle Interfaces: Impact on in Vitro Gastric Stability. Food Hydrocolloids 2018, 84, 282– 291, DOI: 10.1016/j.foodhyd.2018.06.019
12 Eric, D. Colloidal Particles at Liquid Interfaces: Interfacial Particles in Food Emulsions and Foams; Cambridge University Press: Cambridge, 2006.
13 Shi, A.; Feng, X.; Wang, Q.; Adhikari, B. Pickering and High Internal Phase Pickering Emulsions Stabilized by Protein-Based Particles: A Review of Synthesis, Application and Prospective. Food Hydrocolloids 2020, 106117 DOI: 10.1016/j.foodhyd.2020.106117
14 Hu, Z.; Ballinger, S.; Pelton, R.; Cranston, E. D. Surfactant-Enhanced Cellulose Nanocrystal Pickering Emulsions. J. Colloid Interface Sci. 2015, 439, 139– 148, DOI: 10.1016/j.jcis.2014.10.034
15 Beck-Candanedo, S.; Roman, M.; Gray, D. G. Effect of Reaction Conditions on the Properties and Behavior of Wood Cellulose Nanocrystal Suspensions. Biomacromolecules 2005, 6, 1048– 1054, DOI: 10.1021/bm049300p
16 Klemm, D.; Kramer, F.; Moritz, S.; Lindström, T.; Ankerfors, M.; Gray, D.; Dorris, A. Nanocelluloses: A New Family of Nature-Based Materials. Angew. Chem., Int. Ed. 2011, 50, 5438– 5466, DOI: 10.1002/anie.201001273
17 Moon, R. J.; Martini, A.; Nairn, J.; Simonsen, J.; Youngblood, J. Cellulose Nanomaterials Review: Structure, Properties and Nanocomposites. Chem. Soc. Rev. 2011, 40, 3941– 3994, DOI: 10.1039/c0cs00108b
18 Hu, Z.; Patten, T.; Pelton, R.; Cranston, E. D. Synergistic Stabilization of Emulsions and Emulsion Gels with Water-Soluble Polymers and Cellulose Nanocrystals. ACS Sustainable Chem. Eng. 2015, 3, 1023– 1031, DOI: 10.1021/acssuschemeng.5b00194
19 Kalashnikova, I.; Bizot, H.; Cathala, B.; Capron, I. Modulation of Cellulose Nanocrystals Amphiphilic Properties to Stabilize Oil/Water Interface. Biomacromolecules 2012, 13, 267– 275, DOI: 10.1021/bm201599j
20 Kalashnikova, I.; Bizot, H.; Bertoncini, P.; Cathala, B.; Capron, I. Cellulosic Nanorods of Various Aspect Ratios for Oil in Water Pickering Emulsions. Soft Matter 2013, 9, 952– 959, DOI: 10.1039/c2sm26472b
21 Capron, I.; Cathala, B. Surfactant-Free High Internal Phase Emulsions Stabilized by Cellulose Nanocrystals. Biomacromolecules 2013, 14, 291– 296, DOI: 10.1021/bm301871k
22 Li, X.; Li, J.; Gong, J.; Kuang, Y.; Mo, L.; Song, T. Cellulose Nanocrystals (CNCs) with Different Crystalline Allomorph for Oil in Water Pickering Emulsions. Carbohydr. Polym. 2018, 183, 303– 310, DOI: 10.1016/j.carbpol.2017.12.085
23 Capron, I.; Rojas, O. J.; Bordes, R. Behavior of Nanocelluloses at Interfaces. Curr. Opin. Colloid Interface Sci. 2017, 29, 83– 95, DOI: 10.1016/j.cocis.2017.04.001
24 Dai, H.; Wu, J.; Zhang, H.; Chen, Y.; Ma, L.; Huang, H.; Huang, Y.; Zhang, Y. Recent Advances on Cellulose Nanocrystals for Pickering Emulsions: Development and Challenge. Trends Food Sci. Technol. 2020, 102, 16– 29, DOI: 10.1016/j.tifs.2020.05.016
25 Patel, A. R.; Velikov, K. P. Zein as a Source of Functional Colloidal Nano- and Microstructures. Curr. Opin. Colloid Interface Sci. 2014, 19, 450– 458, DOI: 10.1016/J.COCIS.2014.08.001

26 De Folter, J. W. J.; Van Ruijven, M. W. M.; Velikov, K. P. Oil-in-Water Pickering Emulsions Stabilized by Colloidal Particles from the Water-Insoluble Protein Zein. Soft Matter 2012, 8, 6807– 6815, DOI: 10.1039/c2sm07417f
27 Dai, L.; Sun, C.; Wei, Y.; Mao, L.; Gao, Y. Characterization of Pickering Emulsion Gels Stabilized by Zein/Gum Arabic Complex Colloidal Nanoparticles. Food Hydrocolloids 2018, 74, 239– 248, DOI: 10.1016/J.FOODHYD.2017.07.040
28 Wei, Y.; Yu, Z.; Lin, K.; Yang, S.; Tai, K.; Liu, J.; Mao, L.; Yuan, F.; Gao, Y. Fabrication, Physicochemical Stability and Microstructure of Coenzyme Q10 Pickering Emulsions Stabilized by Resveratrol Loaded Composite Nanoparticles. J. Agric. Food Chem. 2020, 68, 1405– 1418, DOI: 10.1021/acs.jafc.9b06678
29 Wei, Y.; Sun, C.; Dai, L.; Zhan, X.; Gao, Y. Structure, Physicochemical Stability and in Vitro Simulated Gastrointestinal Digestion Properties of β-Carotene Loaded Zein-Propylene Glycol Alginate Composite Nanoparticles Fabricated by Emulsification-Evaporation Method. Food Hydrocolloids 2018, 81, 149– 158, DOI: 10.1016/j.foodhyd.2018.02.042
30 Wei, Y.; Zhou, D.; Mackie, A.; Yang, S.; Dai, L.; Zhang, L.; Mao, L.; Gao, Y. Stability, Interfacial Structure, and Gastrointestinal Digestion of β-Carotene-Loaded Pickering Emulsions Co-Stabilized by Particles, a Biopolymer, and a Surfactant. J. Agric. Food Chem. 2021, 69, 1619– 1636, DOI: 10.1021/acs.jafc.0c06409
31 Wei, Y.; Sun, C.; Dai, L.; Mao, L.; Yuan, F.; Gao, Y. Novel Bilayer Emulsions Costabilized by Zein Colloidal Particles and Propylene Glycol Alginate. 2. Influence of Environmental Stresses on Stability and Rheological Properties. J. Agric. Food Chem. 2019, 67, 1209– 1221, DOI: 10.1021/acs.jafc.8b04994
32 Wei, Y.; Tong, Z.; Dai, L.; Ma, P.; Zhang, M.; Liu, J.; Mao, L.; Yuan, F.; Gao, Y. Novel Colloidal Particles and Natural Small Molecular Surfactants Co-Stabilized Pickering Emulsions with Hierarchical Interfacial Structure: Enhanced Stability and Controllable Lipolysis. J. Colloid Interface Sci. 2020, 563, 291– 307, DOI: 10.1016/J.JCIS.2019.12.085
33 Sriamornsak, P.; Thirawong, N.; Cheewatanakornkool, K.; Burapapadh, K.; Sae-Ngow, W. Cryo-Scanning Electron Microscopy (Cryo-SEM) as a Tool for Studying the Ultrastructure during Bead Formation by Ionotropic Gelation of Calcium Pectinate. Int. J. Pharm. 2008, 352, 115– 122, DOI: 10.1016/J.IJPHARM.2007.10.038
34 Li, Y.; McClements, D. J. Inhibition of Lipase-Catalyzed Hydrolysis of Emulsified Triglyceride Oils by Low-Molecular Weight Surfactants under Simulated Gastrointestinal Conditions. Eur. J. Pharm. Biopharm. 2011, 79, 423– 431, DOI: 10.1016/j.ejpb.2011.03.019
35 Li, Y.; Julian McClements, D. New Mathematical Model for Interpreting PH-Stat Digestion Profiles: Impact of Lipid Droplet Characteristics on in Vitro Digestibility. J. Agric. Food Chem. 2010, 58, 8085– 8092, DOI: 10.1021/jf101325m
36 Binks, B. P. Particles as Surfactants—Similarities and Differences. Curr. Opin. Colloid Interface Sci. 2002, 7, 21– 41, DOI: 10.1016/S1359-0294(02)00008-0
37 French, D. J.; Taylor, P.; Fowler, J.; Clegg, P. S. Making and Breaking Bridges in a Pickering Emulsion. J. Colloid Interface Sci. 2015, 441, 30– 38, DOI: 10.1016/J.JCIS.2014.11.032
38 Madivala, B.; Fransaer, J.; Vermant, J. Self-Assembly and Rheology of Ellipsoidal Particles at Interfaces. Langmuir 2009, 25, 2718– 2728, DOI: 10.1021/la803554u
39 Wu, J.; Ma, G. H. Recent Studies of Pickering Emulsions: Particles Make the Difference. Small 2016, 12, 4633– 4648, DOI: 10.1002/smll.201600877
40 Zhang, S.; Holmes, M.; Ettelaie, R.; Sarkar, A. Pea Protein Microgel Particles as Pickering Stabilisers of Oil-in-Water Emulsions: Responsiveness to PH and Ionic Strength. Food Hydrocolloids 2020, 102, 105583 DOI: 10.1016/j.foodhyd.2019.105583

41 MacKie, A.; Gourcy, S.; Rigby, N.; Moffat, J.; Capron, I.; Bajka, B. The Fate of Cellulose Nanocrystal Stabilised Emulsions after Simulated Gastrointestinal Digestion and Exposure to Intestinal Mucosa. Nanoscale 2019, 11, 2991– 2998, DOI: 10.1039/c8nr05860a
42 Wei, Y.; Sun, C.; Dai, L.; Mao, L.; Yuan, F.; Gao, Y. Novel Bilayer Emulsions Costabilized by Zein Colloidal Particles and Propylene Glycol Alginate, Part 1: Fabrication and Characterization. J. Agric. Food Chem. 2019, 67, 1197– 1208, DOI: 10.1021/acs.jafc.8b03240
43 Dickinson, E. Biopolymer-Based Particles as Stabilizing Agents for Emulsions and Foams. Food Hydrocolloids 2017, 68, 219– 231, DOI: 10.1016/J.FOODHYD.2016.06.024
44 Dai, H.; Huang, Y.; Huang, H. Enhanced Performances of Polyvinyl Alcohol Films by Introducing Tannic Acid and Pineapple Peel-Derived Cellulose Nanocrystals. Cellulose 2018, 25, 4623– 4637, DOI: 10.1007/s10570-018-1873-5
45 Dickinson, E. Mixed Biopolymers at Interfaces: Competitive Adsorption and Multilayer Structures. Food Hydrocolloids 2011, 25, 1966– 1983, DOI: 10.1016/j.foodhyd.2010.12.001
46 Wei, Y.; Zhou, D.; Yang, S.; Dai, L.; Zhang, L.; Mao, L. Development of β-Carotene Loaded Oil-in-Water Emulsions Using Mixed Biopolymer–Particle– Development of β-Carotene Loaded Oil-in-Water Surfactant Interfaces. Food Funct. 2021, 12, 3246– 3265, DOI: 10.1039/d0fo02975k
47 Bai, L.; Lv, S.; Xiang, W.; Huan, S.; McClements, D. J.; Rojas, O. J. Oil-in-Water Pickering Emulsions via Microfluidization with Cellulose Nanocrystals: 1. Formation and Stability. Food Hydrocolloids 2019, 96, 699– 708, DOI: 10.1016/j.foodhyd.2019.04.038
48 Bai, L.; Lv, S.; Xiang, W.; Huan, S.; McClements, D. J.; Rojas, O. J. Oil-in-Water Pickering Emulsions via Microfluidization with Cellulose Nanocrystals: 1. Formation and Stability. Food Hydrocolloids 2019, 96, 699– 708, DOI: 10.1016/j.foodhyd.2019.04.038
49 Bai, L.; Lv, S.; Xiang, W.; Huan, S.; McClements, D. J.; Rojas, O. J. Oil-in-Water Pickering Emulsions via Microfluidization with Cellulose Nanocrystals: 2. In Vitro Lipid Digestion. Food Hydrocolloids 2019, 96, 709– 716, DOI: 10.1016/j.foodhyd.2019.04.039
50 Dima, C.; Assadpour, E.; Dima, S.; Jafari, S. M. Bioavailability of Nutraceuticals: Role of the Food Matrix, Processing Conditions, the Gastrointestinal Tract, and Nanodelivery Systems. Compr. Rev. Food Sci. Food Saf. 2020, 19, 954– 994, DOI: 10.1111/1541-4337.12547